JOURNAL OF GUIDANCE, CONTROL, AND DYNAMICS
Vol. 18, No. 3, May–June 1995

Autonomous Imaging of Phobos and Deimos for the PLANET-B Mission

Jun'ichiro Kawaguchi,* Tatsuaki Hashimoto,† Ichiro Nakatani,‡ and Keiken Ninomiya§
Institute of Space and Astronautical Science, Sagamihara, Kanagawa 229, Japan

The Institute of Space and Astronautical Science is currently planning to launch the PLANET-B spacecraft toward Mars, carrying an optical imaging instrument Mars imaging camera, and close-up imaging of Martian satellites Phobos and Deimos is planned. This paper presents analysis of using the optical images as a source in an autonomous, real-time onboard navigation scenario. The results obtained here show that radio metric navigation using ephemerides of Martian satellites will not correctly orient the camera. This paper proposes a nonlinear observer as well as navigation schemes that provide orbital properties in real time such as ballistic parameters and the phase angle in the B-plane (defined as the plane perpendicular to the relative velocity to the target.) Special attention is focused on how the camera angle is programmed in the case of spin-stabilized spacecraft like PLANET-B. Also provided is a new algebraically implemented tracking scheme that is independent of the B-plane properties.

Nomenclature

B = ballistic (or impact) parameter
C_r = projection matrix onto the B-plane
F = system matrix that appears in error propagation
$\boldsymbol{K}$ = Kalman gain matrix
N = number of pixels
$\boldsymbol{n}$ = unit vector normal to $\boldsymbol{V}_{\rm rel}$-Earth direction plane
P = covariance matrix of state or estimation error
R = distance from target object or noise covariance
r = current distance from central body
$\boldsymbol{r}$ = current position vector
$\boldsymbol{s}$ = unit vector in relative velocity direction
T = passage time of closest approach
t = time
$\boldsymbol{v}$ = current velocity vector
$\boldsymbol{V}_{\rm rel}$ = relative velocity vector
$V_{\rm rel}$ = relative velocity
x = navigation parameter, $\boldsymbol{V}_{\rm rel}/B$
$\boldsymbol{x}$ = unit vector perpendicular to both North Pole direction and relative velocity vector
y = cosine of θ_e
$\boldsymbol{y}$ = unit vector normal to both relative velocity vector and $\boldsymbol{x}$ vector in the B plane
z = unit vector in direction of current position vector
α = angle between relative velocity and Earth direction
γ = angle between sun direction and relative velocity
Δt = sampling interval
δ = variation
θ_e = camera elevation angle from spin axis
θ_0 = angle between relative velocity and Earth direction
μ = azimuth angle
ν = width of field of view
τ = time constant
ϕ = angle between closest approach point and current spacecraft position
ϕ_b = phase angle in the B plane
ψ = complementary angle of ϕ

Subscripts

0 = closest approach
$\perp$ = perpendicular state
// = parallel state

Superscripts

$\hat{}$ = estimate
$+$ = postupdate
$-$ = preupdate

I. Introduction

PLANET-B spacecraft departs from Earth in November of 1996 and will be injected into orbit around Mars in September of 1997. Since the primary science goal is plasma physics observations, a highly elliptical orbit is employed whose periapsis altitude is 300 km and apoapsis distance is 10 Martian radii. In addition to plasma physics observation, PLANET-B is going to carry a Mars imaging camera (MIC) to obtain close-up images of Phobos and Deimos from a geophysical point of view.

PLANET-B is a spin-stabilized spacecraft whose spin axis is rigorously pointed toward Earth for the purpose of securing communication. The high-gain antenna is aligned with the spin axis. The spacecraft power system design specifies a retrograde orbit, which makes the relative velocity much higher with respect to the Martian satellites. Figure 1 makes the motivation for this study clear. It illustrates how rapidly camera elevation angle varies when the spacecraft is within a few minute window of the closest approach to the target. Here elevation (aspect) angle is measured from the spin axis. Even the best case requires an orientation shift of 90 deg. In this context, some new concepts are sought to get high-resolution imaging even under such unfavorable conditions. PLANET-B spacecraft images in 512 × 512 pixels with a field of view (FOV) of 11.7 × 11.7 deg. The current specification of MIC onboard is summarized in Table 1.

The orbit of PLANET-B must comply with the scientific requirements, which are incompatible with imaging the Martian satellites. According to the current scenario, the initial inclination angle with respect to the Martian equator is 149 deg, whereas Phobos and Deimos are basically revolving around Mars in circular orbits with inclination of almost zero.

The only way to make PLANET-B closely encounter the Martian satellites is to make the most of secular perturbations that vary the radius of the intersection point between the spacecraft orbit and the Martian equatorial plane. Intersection distance shall be identical to those satellites' distances. PLANET-B's close encounters with Phobos and Deimos during two Earth years are listed in Table 2.

Received Jan. 25, 1994; revision received May 30, 1994; accepted for publication July 18, 1994.

*Associate Professor, Systems Engineering, 3-1-1 Yoshinodai. Member AIAA.
†Research Associate, Spacecraft Control Engineering, 3-1-1 Yoshinodai.
‡Professor, Spacecraft Electrical Systems Engineering, 3-1-1 Yoshinodai.
§Professor, Spacecraft Control Engineering, 3-1-1 Yoshinodai.

Table 1 MIC specification of PLANET-B

Focal length, mm	35, F1.4
Field of view, deg	53 in elevation specified via command
Angular resolution, arc sec	82.6
Number of pixels	2560 (color)
Bit length	8
A/D conversion rate, MHz	6
Frame memory size, Mbyte	1
Weight, kg	less than 2

Table 2 Encounter opportunities with Martian satellites

Name	Date	Relative velocity, km/s	α, deg	γ, deg
1) Deimos	11/5/97	2.2	84.2	112.5
2) Phobos	2/17/98	4.3	134.7	148.3
3) Phobos	3/30/98	4.2	59.1	56.3
4) Deimos	9/9/98	2.2	96.5	76.6

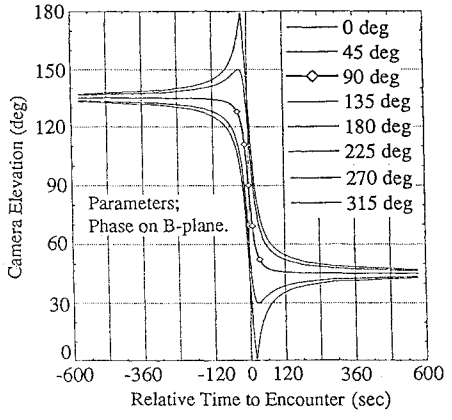

Fig. 1 Camera elevation angle history at the encounter.

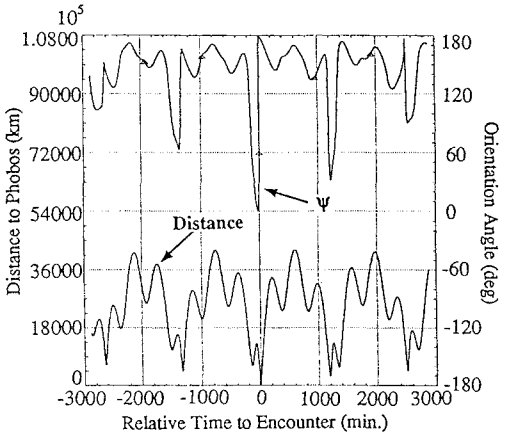

Fig. 2 Distance and orientation angle (Phobos encounter of 1998).

For the Phobos opportunity in February of 1998, Fig. 2 depicts both encounter distance and phase angle ψ (defined in Fig. 4).

As recognized, the flyby speed (expressed via relative velocity) is quite high. The quantity α denotes the elevation angle of the satellites, whereas γ indicates the shadow ratio of the satellites viewed from the spacecraft. When γ is 180 deg, the satellite is at full moon. Phobos in February of 1998 is the best chance, and this case is discussed intensively hereafter.

The assumed exposure plan is summarized in Fig. 3. A few revolutions prior to the closest encounter, the spacecraft is navigated with both radio and optical aid. The nominal exposure sequence has a high-rate exposure of every 10 s, $\pm$10 min with respect to the encounter, whereas just one image is taken every 1 min prior to, as well as after, the encounter.

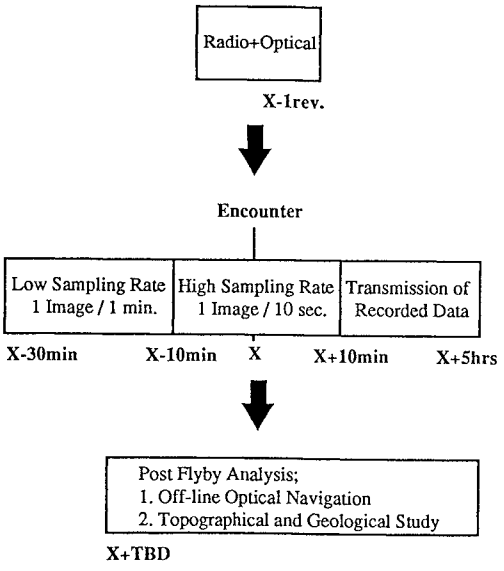

Fig. 3 Imaging plan in PLANET-B mission.

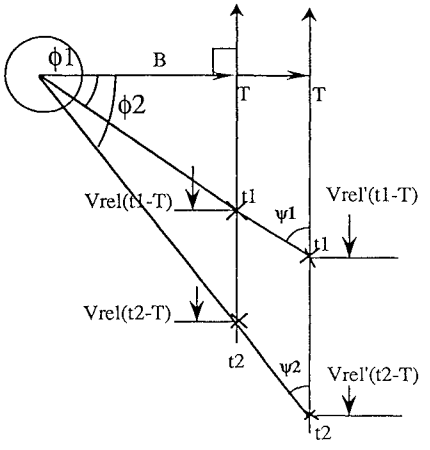

Fig. 4 Linear frozen encounter geometry and optical measurement.

This paper concludes that navigation purely dependent on radio metric measurements with satellite ephemerides is no longer useful during the encounter period. A small nonlinear observer onboard and two kinds of autonomous navigators are proposed, which not only keep tracking but estimate both the ballistic parameter and the phase angle in the B-plane quite well. Finally, a new automated and algebraic scheme is proposed especially for spin-stabilized spacecraft like PLANET-B. Its advantage over other methods is that it excludes any navigation properties and camera orientation is accomplished using only measured elevation angle data.

II. Encounter Geometry and Radio Metric Orbit Determination

Figure 4 is a simplified drawing of a two-body encounter that depicts the resolution constraint. Here ν stands for width of field of view (FOV). Camera orientation error is directly related to ν. If imaging of a satellite is missed during the encounter period due to navigation error δB, the following relation governs:

$$\nu = \frac{2\delta B}{R}$$

Spatial resolution of a camera with FOV ν is

$$\text{res. (Nav.)} = \frac{\nu R}{N(\text{pixel})}$$

Eliminating vR from the equations gives the resultant spatial resolution:

$$\text{res.(Nav.)} = \frac{2\delta B}{N} \tag{1a}$$

which is prescribed by navigation error, whereas the expected spatial resolution is

$$\text{res.(closeup)} = \frac{\text{diameter of object}}{N} \tag{1b}$$

Note this discussion is applicable to either a fixed camera system or a gimbaled camera system without active tracking. The relation in Eq. (1a) is of great importance. The problem arises when the resolution in Eq. (1a) is degraded in comparison with that in Eq. (1b). The ultimate resolution is prescribed by the navigation error rather than camera properties such as focal length or FOV.

A conventional orbit determination process is based on radio metric observations such as range and range rate (R&RR) measurements from ground-based stations. Fundamental error sources governing orbit determination (OD) accuracy are stochastic noise contained in R&RR measurements as well as station location errors. Covariance analysis was carried out to predict OD accuracy at the encounter with Phobos in February of 1998. The results obtained are good with position error of less than 1 km; hence OD accuracy of the spacecraft was not found to be a primary error source. This accuracy can be verified by referring to Ref. 4, where orbital period accuracy of the Viking spacecraft is presented. Once the spacecraft is captured around Mars, relative OD accuracy with respect to Mars is unperturbed by the uncertainty of Mars' ephemeris; therefore a high-precision result is obtained. Reference 5 discusses Phobos' ephemeris accuracy based on the Viking spacecraft for the Phobos mission (USSR). Results there conclude that a 20–40 km uncertainty still remains in spite of the strenuous effort of combining optical observation from Earth and past spacecraft measurements. Such an uncertainty is significant and threatens the close-up imaging here.

If the entire satellite image is to be kept within the FOV even at the closest approach, and considering that the typical size of Martian satellites is 20 km (diameters: Phobos 28 km, Deimos 16 km), the finest resolution intended is approximately 40 m. Since navigation accuracy for the situation described is 20–40 km, imaging without any navigation aid can only guarantee 80–160 m resolution or greater. FOV width at the closest approach distance of 100 km for PLANET-B is determined to be approximately 10 deg. With a 10-deg FOV camera the distance will be 200–400 km, when the satellite becomes lost. This occurs 1–2 min prior to the case of Phobos, in 1998, as the approach velocity is 4.3 km/s. This 1-min period is essential and the key to high-resolution imaging.

III. Optical Navigation Measurement

Figure 4 indicates the basic principle of optical navigation. In a simple situation with two distinct measurements,

$$\tan\phi_1 = x(t_1 - T), \qquad \tan\phi_2 = x(t_2 - T), \qquad x = \frac{V_{\text{rel}}}{B}$$

parameters x and T are determined as

$$x = \frac{\tan\phi_1 - \tan\phi_2}{t_1 - t_2}, \qquad T = \frac{t_2\tan\phi_1 - t_1\tan\phi_2}{\tan\phi_1 - \tan\phi_2} \tag{2}$$

In principle, only parameter x can be obtained and discrimination of B from V_{rel} is hardly possible. This fact may be recognized through Fig. 4, where observations are exactly the same for both trajectories that have different B and V_{rel}. This relation requires that at least V_{rel} should be obtained from other estimation schemes such as radio metric orbit determination, where V_{rel} can be well defined.

In actual application, a series of aspect angle measurements are incorporated so that the most probable impact parameter B can be determined. Each measurement is characterized by

$$z = \frac{r}{r} \tag{3a}$$

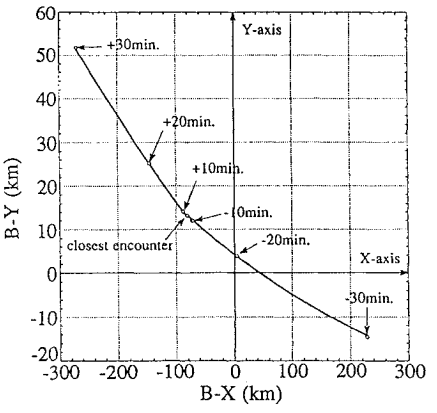

Fig. 5 Impact point in the B-plane (Phobos encounter of 1998).

Since measurement z is related to position error by

$$\delta z = \frac{1}{r}\left(1 - \frac{rr^T}{r^2}\right)\delta r = C_r\delta r \tag{3b}$$

a batch process gives the solution for δr_0:

$$\delta r_0 = \left(\sum_k C_{rk}^T C_{rk}\right)^{-1}\left(\sum_k C_{rk}^T \delta z_k\right) \tag{4}$$

over the accumulated set of measurements.

The actual path is governed by nonlinear orbital dynamics; however, it is not fit for a real-time onboard system as both image processing and navigation computation have to be executed. Throughout this paper, simple dynamics are assumed for the purpose of constructing an onboard system:

$$r = r_0 + v_0(t - t_0)$$
$$r = B_0 + v_0(t - t^*), \qquad B = \left(1 - \frac{v_0 v_0^T}{v_0^2}\right)r_0 \tag{5}$$

The first attempt was done using the batch process [Eq. (4)] together with propagation [Eq. (5)]. However, numerical simulation indicated that it did not function well. The apparent closest approach point defined at each instance never remains constant and is kept almost frozen only during several minutes around the point. The B-plane impact point crosses from the right-hand to left-hand side when the impact point gets extremely small as in Fig. 5. Consequently, it was found that the batch process is not suitable for autonomous orientation, since it is susceptible to an incorrect model.

IV. Observer-Based Tracker

For a high-speed flyby, only sequential navigation can follow a target using the frozen linearized model. The authors have developed a nonlinear observer whose structure is similar to a Kalman filter. The state update and propagation schemes in it are expressed by the following equations:

Nonlinear observer-based tracker:

$$\hat{r}_{k+1}^+ = \hat{r}_{k+1}^- + K_{k+1}\left(z_{k+1} - \frac{\hat{r}_{k+1}^-}{\hat{r}_{k+1}^-}\right)$$
$$\hat{r}_{k+1}^- = \hat{r}_k^+ + v_0\Delta t \tag{6}$$

At the closest passage, the gain is constrained to be small, whereas considerably lower sensitivity at distant locations necessitates higher gain. This situation requires feedback gain to be controlled dependent on estimated states. The quantity δr is expressed as the sum of two distinct components, line of sight (LOS) and that perpendicular to LOS:

$$\delta r = \delta r_\perp + \delta r_{//}$$

In view of the following special property, the projection matrix possesses

$$C_r\delta r_\perp = \frac{1}{r}\delta r_\perp, \qquad C_r\delta r_{//} = 0$$

One strategy is to update the navigation estimates assuming the position error is confined to be perpendicular to the LOS direction, (neglecting errors parallel to it) as

$$\delta\hat{\boldsymbol{r}} = r\delta z \tag{7}$$

And Type-1 gain is proposed here simply utilizing Eq. (7):
Type 1:

$$\boldsymbol{K}_{k+1} \cong \hat{r}_{k+1}^{-} \tag{8}$$

The other choice, Type-2 gain, is obtained taking the Kalman filter structure into account:
Type 2:

$$\boldsymbol{K}_{k+1} \cong \hat{r}_{k+1}^{-2} C_{r,k+1}{}^{T} \tag{9}$$

In a Kalman filter, the gain matrix is calculated via

$$\boldsymbol{K}_{k+1} = P_{k+1}^{-} C_{r,k+1}^{T} \left(R_{k+1} + C_{r,k+1} P_{k+1}^{-} C_{r,k+1}^{T}\right)^{-1} \tag{10}$$

In the case where measurement noise is dominant, the covariance R is approximated as a scalar and, if P is also regarded as a scalar number, the gain matrix may well take the following simple form, where λ is a certain scalar number

$$\boldsymbol{K}_{k+1} = \lambda \cdot C_{r,k+1}^{T} \tag{11}$$

Type-2 gain thus derives from an approximated filter structure. The update process shown in Eq. (6) is rewritten in the following concise form where superscripts $-$ are removed,

$$\hat{\boldsymbol{r}}_{k+1} = \hat{\boldsymbol{r}}_k + \boldsymbol{v}_0 \Delta t + \boldsymbol{K}_k \left(z_k - \frac{\hat{\boldsymbol{r}}_k}{\hat{r}_k}\right) \tag{12}$$

Here the measurement z vector is expanded as

$$\begin{aligned} z_k &= \frac{\boldsymbol{r}_k}{r_k} \cong \frac{\hat{\boldsymbol{r}}_k}{\hat{r}_k} + C_r(\hat{\boldsymbol{r}}_k)(\boldsymbol{r}_k - \hat{\boldsymbol{r}}_k) \\ C_r(\hat{\boldsymbol{r}}_k) &\equiv \frac{1}{\hat{r}_k}\left(1 - \frac{\hat{\boldsymbol{r}}_k \hat{\boldsymbol{r}}_k^{T}}{\hat{r}_k^2}\right) \equiv \frac{1}{\hat{r}_k}\hat{C}_r(\hat{\boldsymbol{r}}_k) \end{aligned} \tag{13}$$

Note the preceding projection matrix has the special property of

$$\hat{C}_r(\hat{\boldsymbol{r}}_k)^2 = \hat{C}_r(\hat{\boldsymbol{r}}_k) \tag{14}$$

Taking advantage of this property, regardless of which type of gain is assumed, the estimated position is obtained by the following computation:

$$\hat{\boldsymbol{r}}_{k+1} \cong \hat{\boldsymbol{r}}_k + \boldsymbol{v}_0 \Delta t + \hat{C}_r(\hat{\boldsymbol{r}}_k)(\boldsymbol{r}_k - \hat{\boldsymbol{r}}_k) \tag{15}$$

For the purpose of assessing estimation error, an error vector is defined:

$$\delta\hat{\boldsymbol{r}}_k \equiv \hat{\boldsymbol{r}}_k - \boldsymbol{r}_k$$

It is found that error propagation is governed by

$$\begin{aligned} \delta\hat{\boldsymbol{r}}_{k+1} &= F(\hat{\boldsymbol{r}}_k)\delta\hat{\boldsymbol{r}}_k + \delta\boldsymbol{v}_0 \Delta t \\ F(\hat{\boldsymbol{r}}_k) &\equiv \frac{\hat{\boldsymbol{r}}_k \hat{\boldsymbol{r}}_k^{T}}{\hat{r}_k^2} \end{aligned} \tag{16}$$

One of the most important things that should be pointed out here is that the error depends on the accuracy of the a priori relative velocity vector $\boldsymbol{v}_0$ that needs to be provided from radio metric navigation in advance. Note that not only the velocity direction but also its magnitude affect the result as well [see Eq. (16)]. Provided $\boldsymbol{v}_0$ information is correct, since

$$P_{k+1}^{-} = P_k^{+}$$

the error covariance matrix P propagates with a measurement noise property characterized by R governed by

$$P_{k+1}^{+} = F(\hat{\boldsymbol{r}}_{k+1}) P_k^{+} F(\hat{\boldsymbol{r}}_{k+1})^{T} + \hat{r}_{k+1}^2 R_{k+1} \tag{17}$$

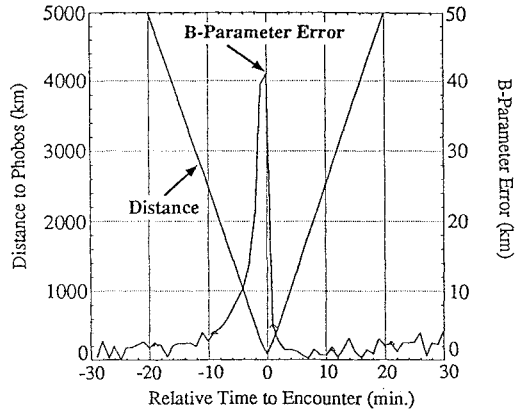

Fig. 6 Distance and B parameter error (observer-based tracker).

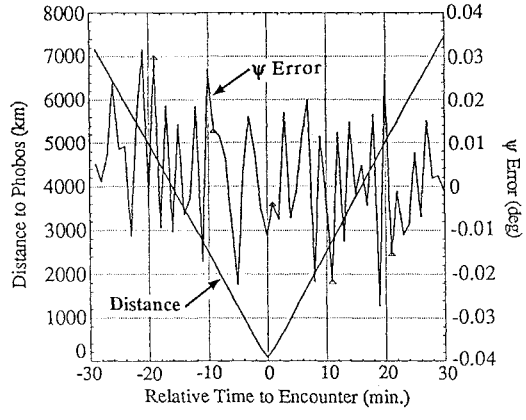

Fig. 7 Distance and orientation angle error (observer-based tracker).

The instantaneous stability of this nonlinear observer [Eq. (6)] is verified by examining eigenvalues of the preceding F matrix. It is easily found that F has two zero eigenvalues and one eigenvalue of unity that corresponds to an eigenvector toward LOS. In other words, the F operator cancels out any position error perpendicular to the LOS direction as follows:

$$\begin{aligned} \delta\hat{\boldsymbol{r}}_{k+1} &= \delta\hat{\boldsymbol{r}}_k - \delta\hat{\boldsymbol{r}}_{k,\perp} + \delta\boldsymbol{v}_0 \Delta t \\ \delta\hat{\boldsymbol{r}}_{k,\perp} &\equiv \hat{C}_r(\hat{\boldsymbol{r}}_k)\delta\hat{\boldsymbol{r}}_k \end{aligned} \tag{18}$$

Note as F is not unstable, P is bounded. At the next measurement step, $k+1$, position vector error projected on the plane perpendicular to LOS vanishes, provided the relative velocity vector is correctly given:

$$\hat{C}_r(\hat{\boldsymbol{r}}_k)\delta\hat{\boldsymbol{r}}_{k+1} = \delta\hat{\boldsymbol{r}}_{k+1,\perp} = \delta\boldsymbol{v}_0 \Delta t \tag{19}$$

Numerical verifications were intensively carried out to examine these nonlinear observers with the aforementioned gains. Figure 6 shows the B-parameter vector error history under Type-1 gain with 1 arc min resolution whose exposure frequency is every 1 min, where initial estimation errors were taken as 5 km for each direction. It implies navigation accuracy is far from adequate, at worst 40 km, when the spacecraft passes at the closest distance. However, the camera tracking capability was found to be good with little error as Fig. 7 shows. Throughout the encounter passage, tracking angle error is kept so small that optical imaging can be continued successfully. The question is why the navigation error builds up to 40 km at the passage in this case, when the initial position error is just 8.7 km (5 km each direction). This is caused mainly by the fact that any observation error is attributed to position error normal to the LOS direction in this formulation. Although the result for Type-2 gain is not shown here, tracking accuracy is similar to that with Type-1 and works efficiently.

V. Self-Governed Algebraic Tracker for Spin-Stabilized Spacecraft

It is assumed that the camera can provide azimuth angle μ as well as elevation (aspect) angle θ_e. And it is also postulated that the spacecraft spin axis coincides with the high-gain antenna aperture that has to be rigorously pointed toward Earth. This is the typical constraint on the attitude of the spin-stabilized spacecraft dealt with here. The situation is depicted in Fig. 8, where the $\boldsymbol{n}$ vector is defined as the unit vector perpendicular to the $\boldsymbol{V}_{\text{rel}}$-$\boldsymbol{E}$ plane and the $\boldsymbol{x}$ axis is taken perpendicular to the $\boldsymbol{V}_{\text{rel}}$-$\boldsymbol{n}$ plane. Note that the $\boldsymbol{n}$ vector is not identical to any North Pole unit vector and $\boldsymbol{x}$-$\boldsymbol{n}$ plane is a kind of B-plane on which the spacecraft path penetrates normally at phase angle ϕ_b. Uncertainty lies primarily in ϕ_b and the time of closest encounter ($t = 0$), whereas the $\boldsymbol{V}_{\text{rel}}$ and $\boldsymbol{E}$ vectors are relatively precisely determined beforehand through radio metric orbit determination. Relative position of spacecraft $\boldsymbol{r}$ is expressed as

$$\boldsymbol{r} = B(\cos\phi_b \cdot \boldsymbol{x} + \sin\phi_b \cdot \boldsymbol{n}) + V_{\text{rel}} \cdot \tau \cdot \boldsymbol{s} \tag{20}$$

Of concern is the elevation angle θ_e of the camera that must be programmed to orient toward the target, whereas the azimuth angle μ is less important for imaging since an automatic trigger capability is given in the PLANET-B spacecraft. The quantity θ_e is expressed as

$$\cos\theta_e = y = -\cos\phi_b \cdot \sin\theta_0 \cdot \cos\phi - \cos\theta_0 \cdot \sin\phi \tag{21}$$

Here ϕ is similarly defined as in Eq. (2) and Fig. 3.

In case Type-1 gain is used, easy manipulation gives Eq. (22) by eliminating relative velocity from Eq. (6),

$$\hat{z}_{k+1}^{-} \cdot \hat{r}_{k+1}^{-} = \hat{z}_k^{-} \cdot \hat{r}_k^{-} + (z_k \cdot r_k^{-} - z_{k-1} \cdot r_{k-1}^{-}) \tag{22}$$

This update rule depicts how the nonlinear observer works here, using extrapolation of the virtual position based on past history. If the preceding expression is examined in the orbital plane, the following relation holds:

$$\tan\hat{\phi}_{k+1} - \tan\hat{\phi}_k = \tan\phi_{k+1} - \tan\phi_k \tag{23}$$

Equation (23) is an extrapolation scheme of tangent ϕ. What is important is that the observer process here is not a pure linear extrapolation of the camera angle but linear in the tangent of the camera angle. This characteristic derives from

$$\frac{\mathrm{d}(\tan\phi)}{\mathrm{d}t} = x \tag{24}$$

Another more important property of y is the relation

$$\frac{\mathrm{d}^2 y}{\mathrm{d}\phi^2} + y = 0 \tag{25}$$

which implies that y (cosine of camera elevation) behaves like harmonic motion in terms of ϕ. Use of Eq. (25) is advantageous since it does not contain ϕ_b explicitly. And elevation orientation is independent of the navigation process. Figure 9 examines this property via numerical simulation confirming the following harmonic relation:

$$y^2 + \left(\frac{\mathrm{d}y}{\mathrm{d}\phi}\right)^2 = \text{const} \tag{26}$$

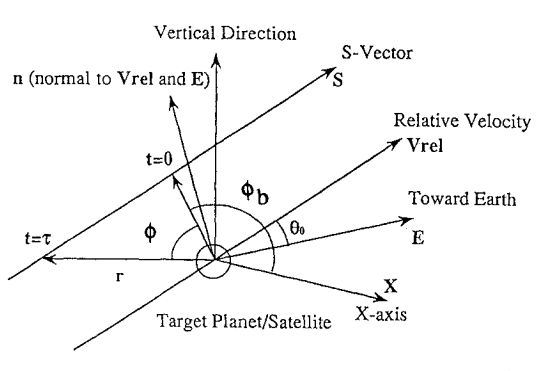

Fig. 8 Imaging geometry in spin-stabilized spacecraft.

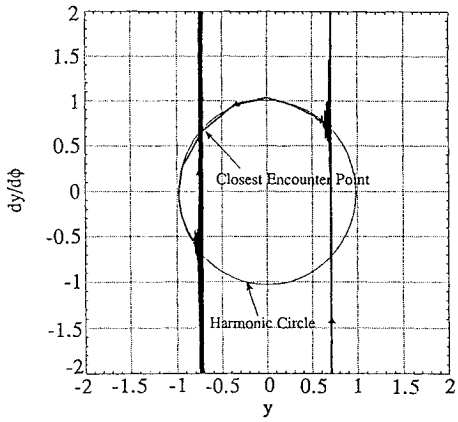

Fig. 9 Harmonic property of elevation angle at the encounter.

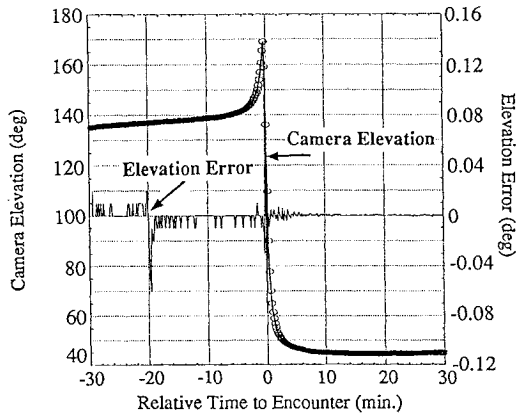

Fig. 10 Camera elevation and elevation error (algebraic tracker).

The solution of Eq. (25) requires two consecutive y measurements that specify elevation at the next instance. Therefore the following algebraic tracker is obtained:

Self-governed algebraic tracker:

$$\hat{\phi}_{k+1} = \tan^{-1}\{2\tan\phi_k - \tan\phi_{k-1}\}$$

$$\cos\hat{\theta}_{e,k+1} = \hat{y}_{k+1} = \frac{\sin(\hat{\phi}_{k+1} - \phi_{k-1})}{\sin(\phi_k - \phi_{k-1})} y_k - \frac{\sin(\hat{\phi}_{k+1} - \phi_k)}{\sin(\phi_k - \phi_{k-1})} y_{k-1} \tag{27}$$

Figure 10 illustrates elevation angle traceability based on this tracker. Although elevation changes up to 120 deg during just 1 min, using this formula keeps the camera perfectly on the target. Any other extrapolation scheme cannot track the target this precisely. Since this formulation does not contain any navigation parameter such as relative velocity vector $\boldsymbol{v}_0$, and the equation itself is in recursive form, this will be the best elevation tracer for a spin-stabilized spacecraft like PLANET-B. The fact that Eq. (27) does not involve $\boldsymbol{v}_0$ and no orbital motion appears in the process means that even poor illumination of the target can be dealt with. It should still be commented that obtaining ϕ information inevitably requires relative velocity direction together with spacecraft attitude. Precisely speaking, relative velocity magnitude never affects camera orientation, whereas relative velocity direction information is needed, even for this scheme. However, Eq. (27) is constructed using the difference of ϕ angles by nature and any bias in the relative velocity vector has little influence on the performance. The other thing to be noted here is that the implementation should avoid division by zero in Eq. (27). Even if ϕ_k is equal to ϕ_{k-1}, Eq. (27) provides that y_{k+1} be equal to y_k as the estimate of ϕ_{k+1} is the same as ϕ_k. Although Eq. (27) is expressed in algebraic form, it requires a few mathematical function tables.

As for circumferential camera orientation, a similar discussion is applied, and the result is obtained as

$$\tan\hat{\mu}_{k+1} = \frac{1}{\tan\phi_k - \tan\phi_{k-1}}\{(\tan\phi_k \cdot \tan\mu_{k-1} - \tan\phi_{k-1} \cdot \tan\mu_k) + (\tan\mu_k - \tan\mu_{k-1}) \cdot \tan\hat{\phi}_{k+1}\} \quad (28)$$

where μ (azimuth angle) is taken from the E-Vertical plane in Fig. 8. Its form also does not contain any navigation quantity. Even though the camera is not equipped with an automatic trigger capability, this formula easily predicts azimuth angle at the next step.

Since y corresponds to the cosine of elevation, if the phase ϕ_b is close to 0 or 180 deg, then the elevation angle θ_e extracted may be quite sensitive to small fluctuations in ϕ. It is because elevation at the closest approach becomes 0 or 180 deg in those situations. (See Fig. 1.) However, this difficulty is not a strict constraint in application. PLANET-B's phase angle in the B-plane is currently planned as 90 or 270 deg. The elevation orientation scheme presented here can take the place of the nonlinear observer [Eq. (6)] concerning autonomous imaging, especially in spin-stabilized spacecraft.

VI. Real-Time Navigators and Onboard System

Differentiating tangent ϕ with respect to time is an easy way to get the navigation property x. A simple way to obtain its estimate is as follows, making use of a low-pass filter:

x-navigator:

$$\hat{x}_{k+1} = \alpha\hat{x}_k + (1-\alpha)q_k$$
$$q_k = [3\tan\phi_k - 4\tan\phi_{k-1} + \tan\phi_{k-2}]/(2\Delta t) \quad (29)$$
$$\alpha = \exp(-\Delta t/\tau_x)$$

where τ_x shall be changed to a sufficiently large figure when tangent ϕ has large values. Typical simulation results are shown in Fig. 11, where the parameter x is estimated from approximately 10 min prior to closest approach. The time constant here is taken as 10 s. Note here that the data interval is every 10 s, whereas the noise property is still left unchanged from previous simulations, with a resolution of 1 arc min.

The method for identifying the navigation property ϕ_b, each time both θ_e and ϕ are obtained is

ϕ_b-navigator:

$$\cos\phi_b = -(\cos\theta_e + \cos\theta_0 \cdot \sin\phi)/(\sin\theta_0 \cdot \cos\phi) \quad (30)$$

This approach leads to an autonomous navigator used in conjunction with the preceding x-navigator. Simulation results are given also in Fig. 11.

A schematic onboard system is shown in Fig. 12 utilizing the algebraic camera tracker [Eq. (27)] together with the aforementioned navigators [Eqs. (29) and (30)].

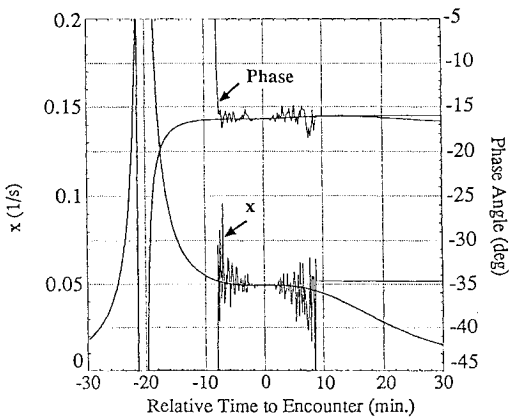

Fig. 11 Navigator outputs (x and phase angle on the B-plane).

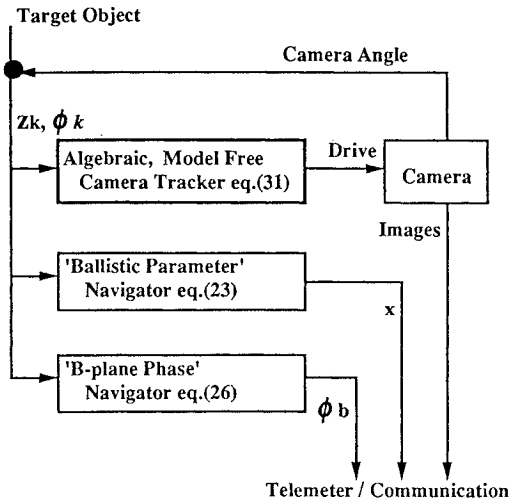

Fig. 12 Onboard software structure—tracker and navigators.

VII. Conclusion

Autonomous imaging of Phobos and Deimos was discussed. The major purpose of the analysis was to establish onboard autonomous navigation software for the PLANET-B mission, which is scheduled to launch in 1996. The problem is guaranteeing optical imaging by ensuring the spacecraft can properly track the object even under an extremely high-speed flyby. Difficulty arose from the fact that scientific requirements specify a retrograde orbit around Mars, which makes flyby speeds quite high. In viewing radio metric navigation accuracy, this paper concluded that the major potential error source lies not in radio metric orbit determination error but in the ephemerides of Phobos and Deimos. It was revealed that this retrograde orbit alters the approach configuration drastically, behaving quite differently from the linear frozen model and a conventional least-square batch process is no longer of practical use.

A sequential nonlinear observer like a Kalman filter was proposed, which keeps tracking throughout a high-speed passage. It may well be referred to as an autonomous tracker based on a navigation aid. It was concluded that even a simplified nonlinear observer can play a prominent role in aligning its LOS direction to the object correctly. Numerical verification was carried out so that low-rate imaging is still capable of exposing a close-up view of those satellites even with the moderate resolution of 1 arc min.

A major drawback of the observer described is its dependency on a priori relative velocity information. A new algebraic tracking scheme driven by a surprisingly simplified recursive form that is perfectly independent of a priori navigation parameters was proposed. Numerical simulation results were shown, which indicate it can track the target very precisely in spite of the rapid motion in elevation angle that moves more than 120 deg during 1 min at closest encounter. This was first proposed in this paper and found quite suitable for spin-stabilized spacecraft like PLANET-B. In addition to those trackers, two kinds of navigator schemes were proposed that estimate x and ϕ_b in real time.

References

[1]Vaughan, R. M., "Optical Navigation for Galileo Gaspra Encounter," AIAA Paper 92-4522, 1990.

[2]Reidel, J., "Optical Navigation During the Voyager Neptune Encounter," AIAA Paper 90-2877, 1990.

[3]Synott, S. P., "Interplanetary Optical Navigation: Voyager Uranus Encounter," AIAA Paper 86-2113, 1986.

[4]Hildebrand, C. E., "Viking Satellite Orbit Determination," *Journal of Guidance and Control*, Vol. 1, No. 6, 1978, pp. 385, 386.

[5]Shor, V. A., "Refinement of the Orbits of Phobos and Deimos Using Ground and Spacecraft Observations," *Soviet Astronomy Letters*, Vol. 14, No. 6, 1988, pp. 477–481.

[6]Ivashkin, V. V., "An Analysis of Characteristics of the Satellite Autonomous Optical Navigation System," International Astronautical Federation, IAF-83-328, Budapest, Hungary, 1983.